This copy is for personal use only. To order printed copies, contact *reprints@rsna.org*

Radiology

Grading of Gliomas by Using Monoexponential, Biexponential, and Stretched Exponential Diffusion-weighted MR Imaging and Diffusion Kurtosis MR Imaging[1]

Yan Bai, MD
Yusong Lin, PhD
Jie Tian, PhD
Dapeng Shi, MD, PhD
Jingliang Cheng, MD, PhD
E. Mark Haacke, PhD
Xiaohua Hong, MD
Bo Ma, MD
Jinyuan Zhou, PhD
Meiyun Wang, MD, PhD

Purpose: To quantitatively compare the potential of various diffusion parameters obtained from monoexponential, biexponential, and stretched exponential diffusion-weighted imaging models and diffusion kurtosis imaging in the grading of gliomas.

Materials and Methods: This study was approved by the local ethics committee, and written informed consent was obtained from all subjects. Both diffusion-weighted imaging and diffusion kurtosis imaging were performed in 69 patients with pathologically proven gliomas by using a 3-T magnetic resonance (MR) imaging unit. An isotropic apparent diffusion coefficient (ADC), true ADC, pseudo-ADC, and perfusion fraction were calculated from diffusion-weighted images by using a biexponential model. A water molecular diffusion heterogeneity index and distributed diffusion coefficient were calculated from diffusion-weighted images by using a stretched exponential model. Mean diffusivity, fractional anisotropy, and mean kurtosis were calculated from diffusion kurtosis images. All values were compared between high-grade and low-grade gliomas by using a Mann-Whitney *U* test. Receiver operating characteristic and Spearman rank correlation analysis were used for statistical evaluations.

Results: ADC, true ADC, perfusion fraction, water molecular diffusion heterogeneity index, distributed diffusion coefficient, and mean diffusivity values were significantly lower in high-grade gliomas than in low-grade gliomas (U = 109, 56, 129, 6, 206, and 229, respectively; $P < .05$). Pseudo-ADC and mean kurtosis values were significantly higher in high-grade gliomas than in low-grade gliomas (U = 98 and 8, respectively; $P < .05$). Both water molecular diffusion heterogeneity index (area under the receiver operating characteristic curve [AUC] = 0.993) and mean kurtosis (AUC = 0.991) had significantly greater AUC values than ADC (AUC = 0.866), mean diffusivity (AUC = 0.722), and fractional anisotropy (AUC = 0.500) in the differentiation of low-grade and high-grade gliomas ($P < .05$).

Conclusion: Water molecular diffusion heterogeneity index and mean kurtosis values may provide additional information and improve the grading of gliomas compared with conventional diffusion parameters.

©RSNA, 2015

Online supplemental material is available for this article.

[1] From the Department of Radiology, Henan Provincial People's Hospital & the People's Hospital of Zhengzhou University, No. 7 Weiwu Road, Zhengzhou, Henan 450003, China (Y.B., D.S., B.M., M.W.); Software Technology School of Zhengzhou University (Y.L.); Institute of Automation, Chinese Academy of Sciences, Beijing, China (J.T.); Division of MRI, First Affiliated Hospital of Zhengzhou University, Zhengzhou Henan, China (J.C.); Department of Radiology, Wayne State University, Detroit, Mich (E.M.H.); Magnetic Resonance Innovations, Detroit, Mich (E.M.H.); and Division of MR Research, Department of Radiology, Johns Hopkins University, Baltimore, Md (X.H., B.M., J.Z., M.W.). Received September 10, 2014; revision requested November 3; revision received February 17, 2015; accepted March 25; final version accepted June 4. Supported in part by the National Natural Science Foundation of China (grants 81271565, 31470047, and 81271534), Distinguished Young Scholar in Scientific and Technical Innovation Foundation of Henan Province, China (grant 124100510016), Science and Technology Foundation of Public Health of Henan Province, China (grants 201202018 and 201003095), and National Clinical Key Specialty of China. **Address correspondence to** M.W. (e-mail: *mywang@ha.edu.cn*).

©RSNA, 2015

Cerebral glioma is the most common type of primary brain tumor and is classified into four grades according to the World Health Organization (WHO) (1). The grading of glioma has clinical significance in determining a treatment strategy and evaluating prognosis. Conventional unenhanced magnetic resonance (MR) imaging and gadolinium-based contrast material–enhanced T1-weighted imaging are usually used to grade gliomas. However, they sometimes fail to provide a reliable prediction of glioma grade because of the overlap of image manifestations in the different grades of gliomas (2,3).

Diffusion MR imaging techniques, such as diffusion-weighted imaging (DWI) and diffusion-tensor imaging, are noninvasive techniques that are sensitive to water molecular diffusion in biological tissue (4,5). An isotropic apparent diffusion coefficient (ADC) obtained from DWI with a monoexponential model, as well as fractional anisotropy (FA) and mean diffusivity obtained from diffusion-tensor imaging, have been used to grade gliomas (4–6). However, contradictory findings about the values of ADC, FA, and mean diffusivity in the grading of gliomas have been reported by several researchers (4–9). ADC values calculated by using a monoexponential model may not be able to accurately reflect water molecular diffusion in vivo, because it is influenced by the microcirculation of blood in capillaries (10). In addition, FA and mean diffusivity values derived from diffusion-tensor imaging by assuming unrestricted and free water diffusion, called Gaussian diffusion distribution, can reflect quantitative information about the direction and magnitude of water molecular diffusion. Yet, the complex microstructures in biological tissue result in hindered and restricted diffusion of water molecules, which leads to a non-Gaussian distribution (11). Thus, FA and mean diffusivity have limitations in the accurate evaluation of water molecular diffusion.

Some previous researchers have suggested that biexponential or stretched exponential DWI models and diffusion kurtosis imaging (DKI) might provide more accurate information about water diffusion (12–14). The biexponential intravoxel incoherent motion DWI model, proposed by Le Bihan et al (12,15), might allow separation of water molecular diffusion from microcirculation. However, its value has not been well explored until recent years. The stretched exponential DWI model, introduced by Bennett et al (13), was used to describe the heterogeneity of intravoxel diffusion rates and the distributed diffusion effect. DKI has been used to measure non-Gaussian diffusion, which has the potential to characterize both normal and pathologic tissue better than diffusion-tensor imaging (16,17). Since DWI with different models and DKI may demonstrate different aspects of tissue properties, it should be valuable to explore and compare their roles in the grading of gliomas. To our knowledge, however, no comparison of these different diffusion imaging approaches in the identification of glioma grade has been investigated so far. The purpose of this study was to quantitatively compare the potential of various diffusion parameters obtained from monoexponential, biexponential, and stretched exponential DWI models and DKI in the grading of gliomas.

Advances in Knowledge

- Except for fractional anisotropy (FA), all the other diffusion parameters were significantly different in high-grade gliomas as compared with low-grade gliomas ($P < .05$), including isotropic apparent diffusion coefficient (ADC), true ADC, pseudo-ADC, and perfusion fraction, calculated from diffusion-weighted imaging (DWI) by using a biexponential model; water molecular diffusion heterogeneity index (α) and distributed diffusion coefficient, calculated from DWI by using a stretched exponential model; and mean diffusivity and mean kurtosis (MK), calculated from diffusion kurtosis images.
- The areas under the receiver operating characteristic curves (AUCs) for both α (AUC = 0.993) and MK (AUC = 0.991) were significantly greater than those of conventional diffusion parameters, including ADC (AUC = 0.866), mean diffusivity (AUC = 0.722), and FA (AUC = 0.500), in the grading of gliomas ($P < .05$).

Implication for Patient Care

- Both α and MK had significantly greater AUC values than ADC, mean diffusivity, and FA in the grading of gliomas ($P < .05$), which may improve the diagnosis and management of gliomas.

Materials and Methods

Patient Population

This prospective study was approved by the local institutional review board.

Published online before print
10.1148/radiol.2015142173 **Content codes:** MR NR

Radiology 2016; 278:496–504

Abbreviations:
ADC = apparent diffusion coefficient
ADC_{fast} = pseudo-ADC
ADC_{slow} = true ADC
AUC = area under the receiver operating characteristic curve
DDC = distributed diffusion coefficient
DKI = diffusion kurtosis imaging
DWI = diffusion-weighted imaging
f = perfusion fraction
FA = fractional anisotropy
MK = mean kurtosis
α = water molecular diffusion heterogeneity index
WHO = World Health Organization

Author contributions:
Guarantors of integrity of entire study, Y.B., B.M., M.W.; study concepts/study design or data acquisition or data analysis/interpretation, all authors; manuscript drafting or manuscript revision for important intellectual content, all authors; approval of final version of submitted manuscript, all authors; agrees to ensure any questions related to the work are appropriately resolved, all authors; literature research, Y.B., D.S., B.M., J.Z., M.W.; clinical studies, Y.B., D.S., B.M., M.W.; experimental studies, Y.B., B.M.; statistical analysis, Y.B., Y.L., J.T., X.H., B.M., M.W.; and manuscript editing, Y.B., Y.L., J.T., D.S., J.C., E.M.H., B.M., J.Z., M.W.

Funding:
This research was supported by the National Institutes of Health (grants R01EB009731 and R01CA166171).

Conflicts of interest are listed at the end of this article.

Written informed consent was obtained from every patient before participation. A total of 69 patients (31 men and 38 women; age range, 25–68 years; mean age, 46 years) with cerebral gliomas that were undergoing MR imaging between April 2012 and May 2014 were enrolled in this study (Table E1 [online]). The inclusion criteria were as follows: *(a)* MR imaging was performed in patients prior to the treatment of gliomas and *(b)* a histopathologic diagnosis based on the WHO 2007 criteria, including astrocytoma, oligodendroglioma, and oligoastrocytoma, was assigned after surgical resection of gliomas within 10 days after the completion of the MR imaging examination. The exclusion criteria were the following: *(a)* MR data were not available owing to head movement artifacts and *(b)* the solid tumor component was unavailable for analysis (<20 mm^2). Finally, five patients with head movement artifacts and two patients with unavailable solid tumor components were excluded, and a total of 62 patients were included.

Image Data Acquisition

All patients underwent imaging by using a 3-T MR imaging unit (Discovery MR 750; GE Medical Systems, Milwaukee, Wis) and an eight-channel head coil (GE Medical Systems).

Conventional MR imaging was performed with a fast spin-echo sequence. Axial T1-weighted images were obtained with a repetition time (msec)/echo time (msec) of 1593/24, while axial T2-weighted images were obtained with 4600/110. Axial T1-weighted sequences were repeated after the intravenous administration of a single dose of gadopentetate dimeglumine (Magnevist; Bayer Schering Pharma, Berlin, Germany).

DWI and DKI were performed before the injection of contrast agents. DWI was performed by using a single-shot echo-planar sequence in the axial plane, 4000/112, section thickness of 4 mm, gap of 0 mm, field of view of 24 × 24 cm, and matrix of 128 × 128. Sixteen b values from 0 to 5000 sec/mm^2 (0, 50, 100, 150, 200, 300, 400, 500, 800, 1000, 1500, 2000, 2500, 3000, 4000, and 5000 sec/mm^2; with one signal acquired for b = 0–800 sec/mm^2, two signals acquired for b = 1000–2000 sec/mm^2, three signals acquired for b = 2500–4000 sec/mm^2, and four signals acquired for b = 5000 sec/mm^2) were used in three diffusion directions. The total acquisition time for DWI, which provided data for monoexponential, biexponential, and stretched exponential model fitting, was 5 minutes 32 seconds. DKI was performed by using six b values that ranged from 0 to 2500 sec/mm^2 (0, 500, 1000, 1500, 2000, and 2500 sec/mm^2, with one signal acquired) with 25 diffusion directions for every b value, 7000/80, section thickness of 4 mm, gap of 0 mm, field of view of 24 × 24 cm, and matrix of 128 × 128. The total acquisition time for DKI was 8 minutes 28 seconds.

According to previous studies (11,18,19), the selections for distributions of b values and numbers of signals acquired in our study are tradeoffs between acquisition times and signal-to-noise ratios in the models. The signal-to-noise ratios in the temporal lobe for b of 5000 sec/mm^2 images in biexponential and stretched exponential models and b of 2500 sec/mm^2 images in the DKI model were calculated to be 12–15 and 19–25, respectively. When compared with some other studies (18,20,21), the signal-to-noise ratios in these diffusion models of our study are reliable even with the highest b values.

Image Data Analysis and Processing

Images were obtained and transferred to a workstation (Advantage Workstation 4.5; GE Medical Systems) for processing. They were independently processed by two neuroradiologists (Y.B. and M.W., who had 7 and 16 years of neurological MR imaging experience, respectively) who were blinded to the histopathologic results.

The ADC value was calculated from all 15 b values by using a monoexponential model as follows (10):

$$S(b)/S(0) = \exp(-b \cdot \mathrm{ADC}),$$

where $S(b)$ represents the signal intensity in the presence of diffusion sensitization and $S(0)$ represents the signal intensity in the absence of diffusion sensitization.

Three parameters—perfusion fraction *(f),* pseudo-ADC ($\mathrm{ADC_{fast}}$), and true ADC ($\mathrm{ADC_{slow}}$)—were calculated by using biexponential intravoxel incoherent motion analysis (10):

$$S(b)/S(0) = [f \cdot \exp(-b \cdot \mathrm{ADC_{fast}})] + [(1-f) \cdot \exp(-b \cdot \mathrm{ADC_{slow}})].$$

By using a stretched exponential DWI model, the water molecular diffusion heterogeneity index (α) and the distributed diffusion coefficient (DDC) were obtained by using the following method (13):

$$S(b)/S(0) = \exp[-(b \cdot \mathrm{DDC})^{\alpha}],$$

where α is related to the intravoxel water molecular diffusion heterogeneity, which varies between 0 and 1. A numerically high α value represents the low intravoxel diffusion heterogeneity (approaching the monoexponential decay). The DDC represents the mean intravoxel diffusion rate.

In addition to FA and mean diffusivity, mean kurtosis (MK) was calculated from DKI. The diffusion kurtosis model is described as follows (16):

$$S(b)/S(0) = \exp\left(-b \cdot D_{\mathrm{app}} + \frac{1}{6} b^2 \cdot D_{\mathrm{app}}{}^2 \cdot K_{\mathrm{app}}\right)$$

and

$$\mathrm{MK} = (1/n)\sum_{i=1}^{n} (K_{\mathrm{app}})_i,$$

where D_{app} is ADC, K_{app} is the K_{app} along the ith direction, and n is the 25 directions in which diffusion measurements are performed. The MK value is derived by averaging all 25 K_{app} values.

In our study, we used the least-squares fit for linear fitting with the monoexponential and DKI models and the Levenberg-Marquardt fit for nonlinear fitting with biexponential and stretched exponential models, which were commonly applied by fitting algorithms in previous studies (Fig 1, *A,* and Fig 2, *A*) (19,22).

Figure 1

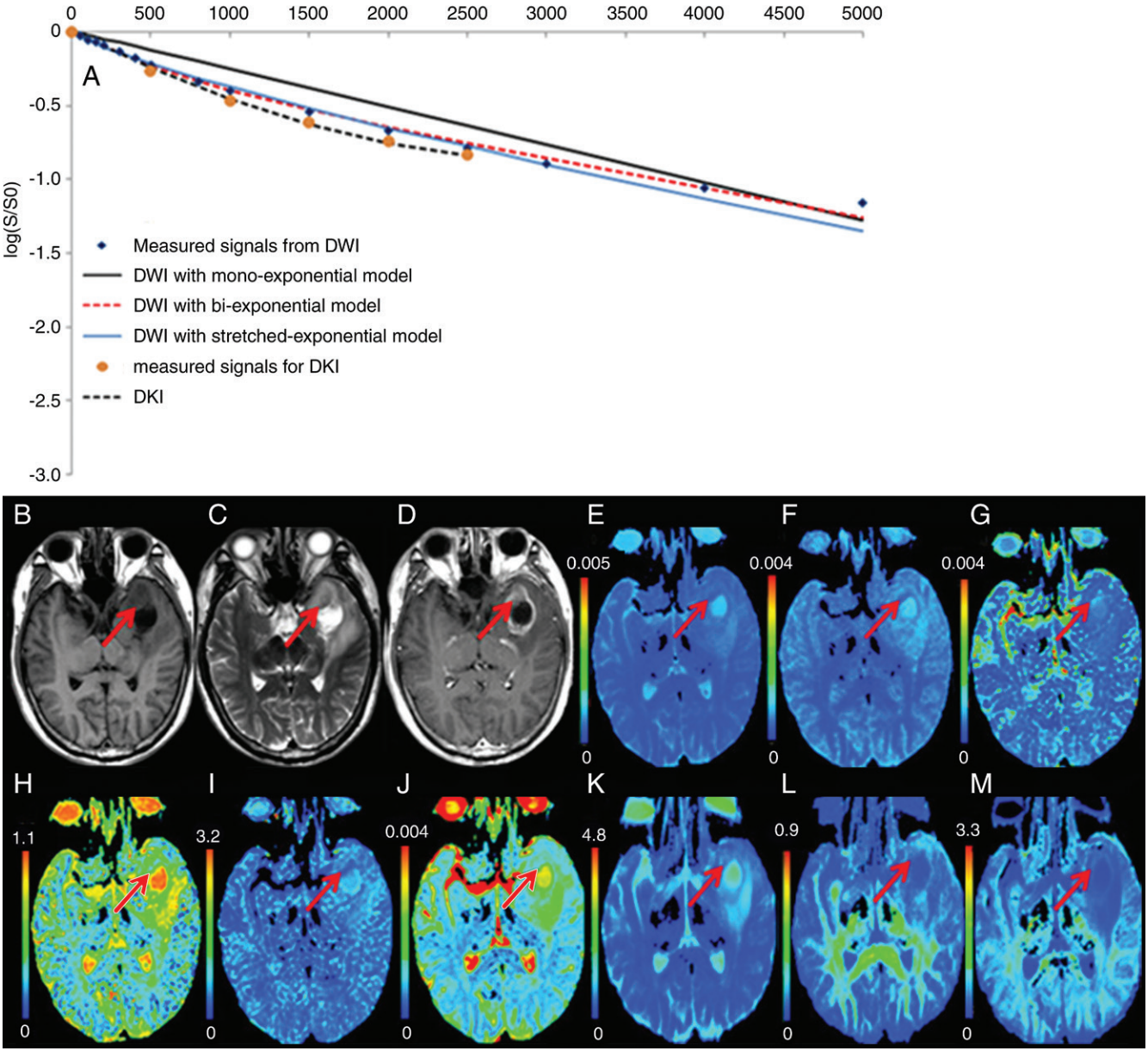

Figure 1: High-grade glioblastoma (WHO grade IV) in the left temporal lobe (arrows) in a 61-year-old woman. *A,* The curves of different fits were derived from DWI by using monoexponential, biexponential, and stretched exponential models and DKI. *B,* T1-weighted MR image shows that the tumor is hypointense. *C,* T2-weighted MR image shows that the tumor is hyperintense. *D,* Gadolinium-based contrast material–enhanced T1-weighted MR image shows that the tumor has irregular enhancement. In the solid tumor component that enhances with gadolinium-based contrast material, *E,* the ADC map and, *F,* the ADC_{slow} map show decreased values. *G,* The ADC_{fast} map shows increased values, and, *H,* the *f* map, *I,* α map, *J,* DDC map, and, *K,* mean diffusivity map show decreased values. The, *L,* FA and, *M,* MK maps show increased values.

The two blinded neuroradiologists (Y.B. and M.W.) analyzed all the images independently. For every patient, each neuroradiologist placed three regions of interest in the different solid tumor components within white matter on the ADC maps to obtain measurements. The areas of the regions of interest varied from 20 to 45 mm^2 (mean area, 37 mm^2), and areas of necrosis, cyst, hemorrhage, large vessels, edema, and calcifications were avoided to ensure more accurate measurements. Then, the selected regions of interest with the lowest mean ADC values on ADC maps

Figure 2

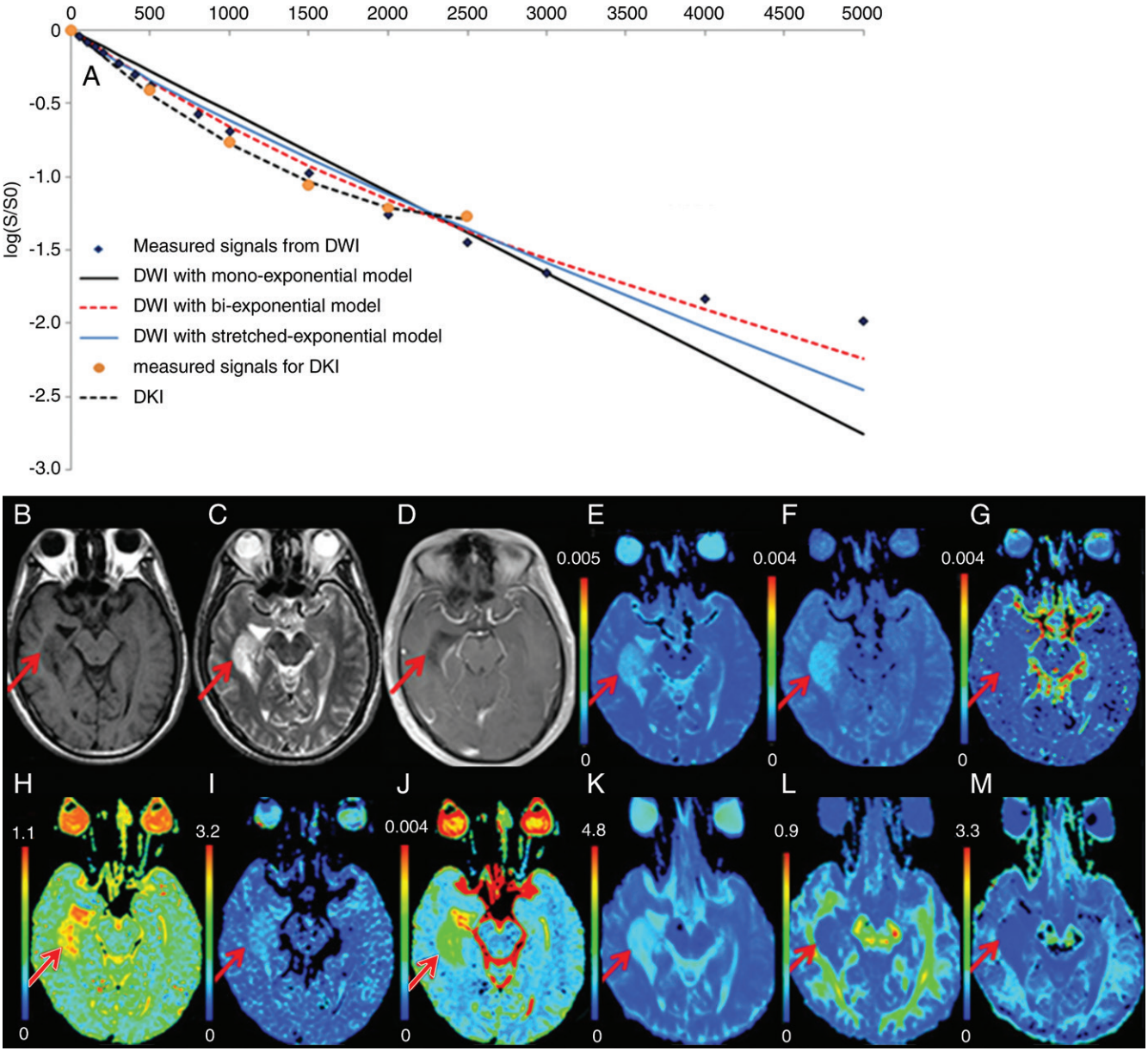

Figure 2: Low-grade astrocytoma (WHO grade II) in the right temporal lobe (arrows) in a 43-year-old woman. *A,* The curves of different fits were derived from DWI by using monoexponential, biexponential, and stretched exponential models and DKI. *B,* T1-weighted MR image shows that the tumor is hypointense. *C,* T2-weighted MR image shows that the tumor is hyperintense. *D,* Gadolinium-based contrast-enhanced T1-weighted MR image shows that the tumor has no enhancement. In the tumor, *E,* the ADC map and, *F,* the ADC_{slow} map show increased values. *G,* The ADC_{fast} map shows decreased values. The, *H, f* map, *I,* α map, *J,* DDC map, and, *K,* mean diffusivity map show increased values. The, *L,* FA and, *M,* MK map show decreased values.

were copied to the maps of all the other parameters from the same patient.

Statistical Analysis

All statistical analyses were performed with SPSS software (version 17.0; SPSS, Chicago, Ill). The mean results of each parameter for each subject according to the two radiologists were used for quantitative statistical analyses. The Mann-Whitney *U* test was used for the comparison of each parameter between high-grade and low-grade gliomas. The Wilcoxon signed rank test was used to compare ADC and ADC_{slow} values calculated from all subjects. Results with *P* values less than .05 were considered to indicate a significant difference.

Correlations among all parameters were assessed by using Spearman rank correlation. Sidak corrections (with a 0.95 confidence level), which can reduce the type I error, were used for multiple comparisons. Receiver operating characteristic curves were generated for each parameter to assess the area under the receiver operating characteristic curve (AUC) and to determine which parameter was optimal for the grading of gliomas. The cutoff points were selected by using the maximized values of the Youden indexes. Then, the sensitivity and specificity at the threshold values for each diffusion parameter were determined in the grading of gliomas. Interrater reliability between the two independent quantitative analyses was assessed by using an intraclass correlation coefficient. Results with *P* values less than .05 were considered to indicate a significant difference.

Results

Thirty-four of 62 patients (55%) were confirmed with pathologic examination to have high-grade (WHO grades III and IV) gliomas, and the remaining 28 patients (45%) had low-grade (WHO grade II) gliomas. The diagnoses of the patient group included WHO grade II astrocytomas (n = 15), grade II oligodendrogliomas (n = 8), grade II oligoastrocytomas (n = 5), grade III anaplastic astrocytomas (n = 8), grade III anaplastic oligodendrogliomas (n = 2), grade III anaplastic oligoastrocytomas (n = 5), and grade IV glioblastomas (n = 19).

Thirty of 34 high-grade gliomas (88%) and six of 28 low-grade gliomas (21%) demonstrated enhancement on the contrast-enhanced T1-weighted images. For the two radiologists (Y.B. and M.W.), the respective sensitivity and specificity for conventional MR imaging were 73.5% (25 of 34 gliomas) and 67.8% (19 of 28 gliomas) for Y.B. and 76.4% (26 of 34 gliomas) and 71.4% (20 of 28 gliomas) for M.W. in the determination of high-grade gliomas.

Figure 1, *B–M,* and Figure 2, *B–M,* show the manifestations of high- and low-grade gliomas on T1- and T2-weighted images, gadolinium-based contrast material–enhanced T1-weighted images, and ADC, ADC_{fast}, ADC_{slow}, *f,* α, DDC, mean diffusivity, FA, and MK maps. Figure 3 shows the quantitative comparison of differences in diffusion parameters between the two glioma groups. ADC, ADC_{slow}, *f,* α, DDC, and mean diffusivity values were significantly lower in high-grade gliomas than in low-grade gliomas ($P < .05$). Additionally, ADC_{fast} and MK were significantly higher in high-grade gliomas than in low-grade gliomas ($P < .05$). However, FA did not show a significant difference between the two groups ($P > .05$).

Figure 3

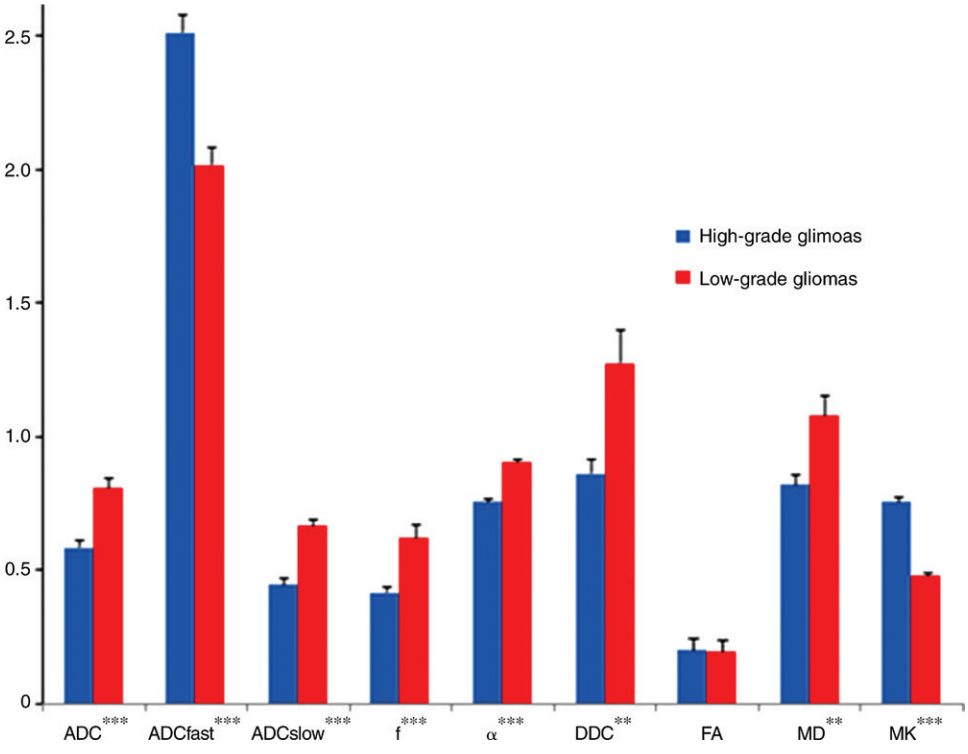

Figure 3: Bar graphs of ADC, ADC_{fast}, ADC_{slow}, *f,* α, DDC, FA, mean diffusivity *(MD),* and MK values averaged across high-grade (n = 34) and low-grade (n = 28) gliomas. Error bars = standard deviations across subjects. ADC, ADC_{fast}, ADC_{slow}, DDC, and MD are in units of $\times 10^{-3}$ mm^2/sec. Parameters not marked with asterisks are not significant. ** = $P < .01$, *** = $P < .001$.

ADC_{slow} was significantly lower than ADC in all subjects ($P < .05$).

When looking at the receiver operating characteristic curves in discriminating high-grade gliomas from low-grade gliomas (Fig 4), AUC values were 0.993 for α, 0.991 for MK, 0.939 for ADC_{slow}, 0.900 for ADC_{fast}, 0.866 for ADC, 0.782 for DDC, 0.722 for mean diffusivity, and 0.500 for FA. The AUC values for both α and MK were significantly greater than those for ADC, mean diffusivity, and FA in the grading of gliomas ($P < .05$). Table 1 shows the sensitivity and specificity of diffusion parameters at optimal cutoff values in differentiating low-grade from high-grade gliomas.

The quantitative correlation analysis showed that there were strong correlations between ADC and ADC_{slow}, ADC_{fast}, *f*, α, mean diffusivity, and MK ($P < .001$) (Table 2). After Sidak corrections for multiple comparisons, MK correlated with all the other parameters ($P < .001$) except FA ($P > .05$). In particular, there was a strong negative correlation between MK and α in gliomas ($r = -0.742$, $P < .001$).

The overall mean intraclass correlation coefficient between the two independent radiologists was 0.873 ($P < .001$).

Figure 4

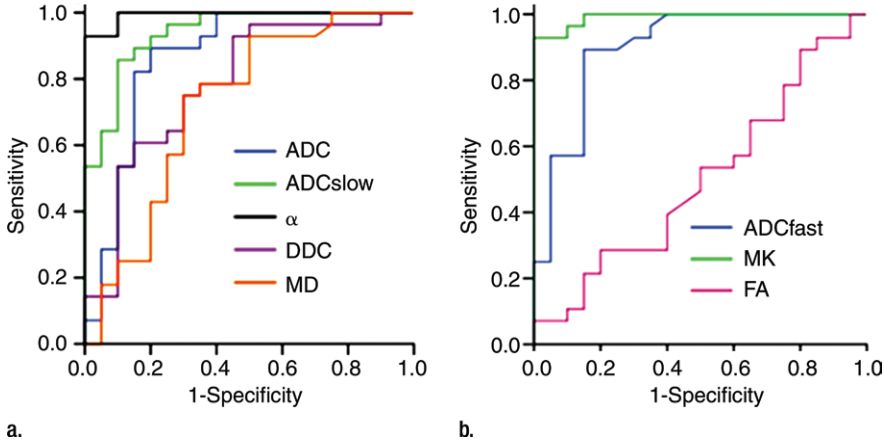

Figure 4: **(a)** Receiver operating characteristic curves for ADC, ADC_{slow}, α, DDC, and mean diffusivity *(MD)* in distinguishing high- from low-grade gliomas. **(b)** Receiver operating characteristic curves for ADC_{fast}, MK, and FA in distinguishing high- from low-grade gliomas.

Table 1

Sensitivity and Specificity of Diffusion Parameters at Optimal Cutoff Values in Differentiating Low- from High-Grade Gliomas

Diffusion Parameter	Optimal Cutoff Value	Sensitivity (%)	Specificity (%)
ADC	0.696*	89.3 (25/28)	79.4 (27/34)
ADC_{fast}	2.215*	89.3 (25/28)	85.3 (29/34)
ADC_{slow}	0.552*	85.7 (24/28)	91.2 (31/34)
α	0.813	92.9 (26/28)	100 (34/34)
DDC	0.896*	60.7 (17/28)	85.3 (29/34)
FA	0.062	89.3 (25/28)	20.6 (7/34)
Mean diffusivity	0.937*	78.6 (22/28)	64.7 (22/34)
MK	0.616	92.9 (26/28)	100 (34/34)

Note.—Numbers in parentheses are the data used to calculate percentages.
* Values are in units of $\times 10^{-3}$ mm^2/sec.

Discussion

In this study, our results showed that both α and MK had significantly greater diagnostic properties than did conventional diffusion parameters, including ADC, mean diffusivity, and FA, in differentiating low-grade gliomas from high-grade gliomas. As such, MK may serve as an optimal diffusion parameter for grading gliomas in clinical practice.

One previous study on DWI in the evaluation of cellularity in gliomas reported by Sugahara et al (4) and another study on the neuropathologic diagnosis of brain tumors reported by Pollo (23) demonstrated that both tumor cellularity and vascularity were higher in high-grade gliomas than in low-grade gliomas. Since high tumor cellularity can decrease ADC values, whereas the high vascularity may increase the ADC (4,10,12), the DWI signal attenuation may be affected in opposite ways. Thus, ADC calculated from the monoexponential model is limited in grading gliomas, leading to contradictory results (4,6,7,24,25). However, ADC_{slow} derived from biexponential intravoxel incoherent motion can remove the influence of perfusion, so it may reflect the true diffusion coefficient.

Perfusion parameters, such as cerebral blood flow and cerebral blood volume, have previously been shown to be helpful in grading gliomas (3,26). Previous studies (27,28) showed that ADC_{fast} and *f* were associated with perfusion quantitatively in the human brain. The results of our current study showed that ADC_{fast} was significantly higher in high-grade gliomas than in low-grade gliomas, whereas *f* was significantly higher in low-grade gliomas than in high-grade gliomas. These current results were consistent with the findings from previous studies (3,26,29,30).

The discordance between *f* and other perfusion parameters obtained by using contrast media may be caused by differences in imaging techniques (29). Furthermore, water molecules are less restricted in the relatively larger extracellular space in a low-grade glioma (4), which may contribute to the increase of the fast diffusion fraction. However, Sehy et al (31) reported that fast

Table 2

Spearman Rank Correlation Coefficients between DWI and DKI Measurements

Parameter	ADC Value	ADC_{fast} Value	ADC_{slow} Value	*f* Value	α Value	DDC Value	FA Value	Mean Diffusivity
ADC_{fast}	−0.480*	…	…	…	…	…	…	…
ADC_{slow}	0.786*	−0.492*	…	…	…	…	…	…
f	0.874*	−0.419	0.713*	…	…	…	…	…
α	0.684*	−0.669*	0.871*	0.625*	…	…	…	…
DDC	0.834*	−0.217	0.754*	0.897*	0.621*	…	…	…
FA	−0.306	−0.175	−0.214	−0.342	−0.184	−0.246	…	…
Mean diffusivity	0.709*	−0.427	0.523*	0.709*	0.449*	0.596*	−0.297	…
MK	−0.720*	0.638*	−0.685*	−0.612*	−0.742*	−0.513*	0.221	−0.559*

Note.—Values not marked with a footnote are not significant.

* Value is significant with Sidak corrections for multiple comparisons ($P < .001$).

diffusion fraction could arise from the intracellular space of the *Xenopus* oocyte. However, in another study by Sehy et al (32), the authors mentioned the importance of noting that restrictions of water motion due to the presence of cell membranes were more prominent in mammalian brains than in oocytes. As compared with glioma cells (33), the ADC values may increase in the intracellular space of oocytes because of the larger cell sizes (32), which contributes to fast diffusion fraction.

The stretched exponential model can overcome the limitations of the hypothesis about fast and slow diffusion compartments and the slow exchange between them in a biexponential model. DDC can be considered the composite of individual ADCs, weighted by the volume fraction of water molecules in each part of the continuous distribution of ADCs (34). A previous study demonstrated that the heterogeneity index of high-grade gliomas was significantly different from that of normal brain structures (19). Our current results demonstrated that α was significantly lower in high-grade gliomas than in low-grade gliomas. One possible explanation of our findings is that high-grade gliomas exhibit more intravoxel diffusion heterogeneity than low-grade gliomas because they possess more histologic heterogeneity, such as heterogeneous cellularity and tortuous vascular hyperplasia (35). Some other previous studies have shown that FA and mean diffusivity derived from diffusion-tensor imaging were not consistently helpful in the grading of gliomas (8,9), since diffusion-tensor imaging might not be accurate enough to reflect the actual non-Gaussian diffusion distribution in biological tissue. As an extension of diffusion-tensor imaging, DKI can provide an additional measurement, MK, to characterize the complexity of the microenvironment and has the potential to allow measurement of the non-Gaussian diffusion in biological tissue. On the basis of our results, MK showed better separation between high- and low-grade gliomas than FA and mean diffusivity, which was in agreement with some recent studies (9,11).

It is thought that α may reflect microstructural heterogeneity (13), and MK may indicate microstructural complexity (9). Although the exact meanings of α and MK in vivo are still not fully understood (9,22), the strong correlation between them in gliomas in our current results suggest that α and MK may be similar in demonstrating the pathologic characteristics of gliomas.

This study had some limitations. First, the patient population was relatively small, and the subtypes of gliomas were not evaluated. Second, the regions of interest were selected in the solid parts of the tumors instead of the entire gliomas in this study, which might lead to some selection bias owing to the histologic heterogeneity of gliomas. In the future, the association of different DWI models and DKI with the detailed histologic characteristics should be investigated further.

In conclusion, our results suggest that α and MK may provide additional information for the grading of gliomas compared with conventional diffusion parameters, which would be helpful in improving therapy strategies and prognoses.

Acknowledgments: The authors thank Mary McAllister, MA, in the Department of Radiology at Johns Hopkins University, Baltimore, Maryland, for editorial assistance; Zhenyu Zhou, PhD, Dandan Zheng, PhD, and Fei Sun, PhD, at GE Healthcare, Beijing, China, for technical support; and Yong Zhang, PhD, at GE Healthcare, Shanghai, China, for technical support.

Disclosures of Conflicts of Interest: Y.B. disclosed no relevant relationships. **Y.L.** disclosed no relevant relationships. **J.T.** disclosed no relevant relationships. **D.S.** disclosed no relevant relationships. **J.C.** disclosed no relevant relationships. **E.M.H.** disclosed no relevant relationships. **X.H.** disclosed no relevant relationships. **B.M.** disclosed no relevant relationships. **J.Z.** disclosed no relevant relationships. **M.W.** disclosed no relevant relationships.

References

1. Louis DN, Ohgaki H, Wiestler OD, et al. The 2007 WHO classification of tumours of the central nervous system. Acta Neuropathol (Berl) 2007;114(2):97–109.
2. Scott JN, Brasher PM, Sevick RJ, Rewcastle NB, Forsyth PA. How often are nonenhancing supratentorial gliomas malignant? A population study. Neurology 2002;59(6):947–949.
3. Law M, Young R, Babb J, et al. Comparing perfusion metrics obtained from a single compartment versus pharmacokinetic modeling methods using dynamic susceptibility

contrast-enhanced perfusion MR imaging with glioma grade. AJNR Am J Neuroradiol 2006;27(9):1975–1982.

4. Sugahara T, Korogi Y, Kochi M, et al. Usefulness of diffusion-weighted MRI with echo-planar technique in the evaluation of cellularity in gliomas. J Magn Reson Imaging 1999;9(1):53–60.
5. Stadlbauer A, Ganslandt O, Buslei R, et al. Gliomas: histopathologic evaluation of changes in directionality and magnitude of water diffusion at diffusion-tensor MR imaging. Radiology 2006;240(3):803–810.
6. Kang Y, Choi SH, Kim YJ, et al. Gliomas: histogram analysis of apparent diffusion coefficient maps with standard- or high-b-value diffusion-weighted MR imaging—correlation with tumor grade. Radiology 2011; 261(3):882–890.
7. Lam WW, Poon WS, Metreweli C. Diffusion MR imaging in glioma: does it have any role in the pre-operation determination of grading of glioma? Clin Radiol 2002;57(3):219–225.
8. Lee HY, Na DG, Song IC, et al. Diffusion-tensor imaging for glioma grading at 3-T magnetic resonance imaging: analysis of fractional anisotropy and mean diffusivity. J Comput Assist Tomogr 2008;32(2):298–303.
9. Van Cauter S, Veraart J, Sijbers J, et al. Gliomas: diffusion kurtosis MR imaging in grading. Radiology 2012;263(2):492–501.
10. Le Bihan D, Breton E, Lallemand D, Aubin ML, Vignaud J, Laval-Jeantet M. Separation of diffusion and perfusion in intravoxel incoherent motion MR imaging. Radiology 1988;168(2):497–505.
11. Raab P, Hattingen E, Franz K, Zanella FE, Lanfermann H. Cerebral gliomas: diffusional kurtosis imaging analysis of microstructural differences. Radiology 2010;254(3):876–881.
12. Le Bihan D, Breton E, Lallemand D, Grenier P, Cabanis E, Laval-Jeantet M. MR imaging of intravoxel incoherent motions: application to diffusion and perfusion in neurologic disorders. Radiology 1986;161(2):401–407.
13. Bennett KM, Schmainda KM, Bennett RT, Rowe DB, Lu H, Hyde JS. Characterization of continuously distributed cortical water diffusion rates with a stretched-exponential model. Magn Reson Med 2003;50(4):727–734.
14. De Santis S, Gabrielli A, Palombo M, Maraviglia B, Capuani S. Non-Gaussian diffusion imaging: a brief practical review. Magn Reson Imaging 2011;29(10):1410–1416.
15. Le Bihan D. Intravoxel incoherent motion perfusion MR imaging: a wake-up call. Radiology 2008;249(3):748–752.
16. Jensen JH, Helpern JA, Ramani A, Lu H, Kaczynski K. Diffusional kurtosis imaging: the quantification of non-Gaussian water diffusion by means of magnetic resonance imaging. Magn Reson Med 2005;53(6):1432–1440.
17. Lu H, Jensen JH, Ramani A, Helpern JA. Three-dimensional characterization of non-Gaussian water diffusion in humans using diffusion kurtosis imaging. NMR Biomed 2006;19(2):236–247.
18. Zhou XJ, Gao Q, Abdullah O, Magin RL. Studies of anomalous diffusion in the human brain using fractional order calculus. Magn Reson Med 2010;63(3):562–569.
19. Kwee TC, Galbán CJ, Tsien C, et al. Intravoxel water diffusion heterogeneity imaging of human high-grade gliomas. NMR Biomed 2010;23(2):179–187.
20. Jones DK. The effect of gradient sampling schemes on measures derived from diffusion tensor MRI: a Monte Carlo study. Magn Reson Med 2004;51(4):807–815.
21. Gao Y, Zhang Y, Wong CS, et al. Diffusion abnormalities in temporal lobes of children with temporal lobe epilepsy: a preliminary diffusional kurtosis imaging study and comparison with diffusion tensor imaging. NMR Biomed 2012;25(12):1369–1377.
22. Yuan J, Yeung DK, Mok GS, et al. Non-Gaussian analysis of diffusion weighted imaging in head and neck at 3T: a pilot study in patients with nasopharyngeal carcinoma. PLoS ONE 2014;9(1):e87024.
23. Pollo B. Neuropathological diagnosis of brain tumours. Neurol Sci 2011;32(2 Suppl 2): S209–S211.
24. Rollin N, Guyotat J, Streichenberger N, Honnorat J, Tran Minh VA, Cotton F. Clinical relevance of diffusion and perfusion magnetic resonance imaging in assessing intraaxial brain tumors. Neuroradiology 2006; 48(3):150–159.
25. Di Costanzo A, Scarabino T, Trojsi F, et al. Multiparametric 3T MR approach to the assessment of cerebral gliomas: tumor extent and malignancy. Neuroradiology 2006; 48(9):622–631.
26. Mills SJ, Patankar TA, Haroon HA, Balériaux D, Swindell R, Jackson A. Do cerebral blood volume and contrast transfer coefficient predict prognosis in human glioma? AJNR Am J Neuroradiol 2006;27(4):853–858.
27. Wirestam R, Borg M, Brockstedt S, Lindgren A, Holtås S, Ståhlberg F. Perfusion-related parameters in intravoxel incoherent motion MR imaging compared with CBV and CBF measured by dynamic susceptibility-contrast MR technique. Acta Radiol 2001; 42(2):123–128.
28. Federau C, Maeder P, O'Brien K, Browaeys P, Meuli R, Hagmann P. Quantitative measurement of brain perfusion with intravoxel incoherent motion MR imaging. Radiology 2012;265(3):874–881.
29. Sumi M, Nakamura T. Head and neck tumors: assessment of perfusion-related parameters and diffusion coefficients based on the intravoxel incoherent motion model. AJNR Am J Neuroradiol 2013;34(2):410–416.
30. Ganten MK, Schuessler M, Bäuerle T, et al. The role of perfusion effects in monitoring of chemoradiotherapy of rectal carcinoma using diffusion-weighted imaging. Cancer Imaging 2013;13(4):548–556.
31. Sehy JV, Ackerman JJ, Neil JJ. Evidence that both fast and slow water ADC components arise from intracellular space. Magn Reson Med 2002;48(5):765–770.
32. Sehy JV, Zhao L, Xu J, Rayala HJ, Ackerman JJ, Neil JJ. Effects of physiologic challenge on the ADC of intracellular water in the Xenopus oocyte. Magn Reson Med 2004;52(2):239–247.
33. Ko L, Koestner A, Wechsler W. Morphological characterization of nitrosourea-induced glioma cell lines and clones. Acta Neuropathol (Berl) 1980;51(1):23–31.
34. Bennett KM, Hyde JS, Schmainda KM. Water diffusion heterogeneity index in the human brain is insensitive to the orientation of applied magnetic field gradients. Magn Reson Med 2006;56(2):235–239.
35. Behin A, Hoang-Xuan K, Carpentier AF, Delattre JY. Primary brain tumours in adults. Lancet 2003;361(9354):323–331.